

Article

Ion-Exchange of Cu^{2+} Promoted Layered Perovskite $\text{K}_2\text{La}_2\text{Ti}_3\text{O}_{10}$ for Photocatalytic Degradation Chlorobenzene under Simulated Solar Light Irradiation

Dandan Pang, Jie Gao, Feng Ouyang *, Rongshu Zhu and Charlene Xie

Shenzhen Key Laboratory of Organic Pollution Prevention and Control, Shenzhen Graduate School, Harbin Institute of Technology, Shenzhen 518055, China; ddpang1221@foxmail.com (D.P.); ningmenghit@163.com (J.G.); rszhulit@hit.edu.cn (R.Z.); charlenexie@hit.edu.cn (C.X.)

* Correspondence: ouyangfh@hit.edu.cn; Tel.: +86-755-2603-3472

Academic Editors: Shaobin Wang and Xiaoguang Duan

Received: 26 February 2017; Accepted: 21 April 2017; Published: 26 April 2017

Abstract: The layered perovskite, $\text{K}_2\text{La}_2\text{Ti}_3\text{O}_{10}$ was prepared by sol-gel method. Ion-exchange of Cu^{2+} was prepared to improve the photocatalytic activity of $\text{K}_2\text{La}_2\text{Ti}_3\text{O}_{10}$ for chlorobenzene degradation under simulated solar light irradiation. The original $\text{K}_2\text{La}_2\text{Ti}_3\text{O}_{10}$ and $\text{Cu}^{2+}/\text{K}_2\text{La}_2\text{Ti}_3\text{O}_{10}$ were characterized by power X-ray diffraction, UV-visible diffuse reflectance spectroscopy, and specific surface area measurement. The XRD analysis shows that Cu^{2+} ions is incorporated in place of K^+ ions and the grain growth is inhibited by ion-exchange. With the rise of calcination temperature, more interlayer Cu^{2+} was converted into new crystal phase CuO . The degradation ratio reaches 51.1% on $\text{Cu}^{2+}/\text{K}_2\text{La}_2\text{Ti}_3\text{O}_{10}$ calcined at 500 °C in air, which is higher 16.9% than the original $\text{K}_2\text{La}_2\text{Ti}_3\text{O}_{10}$. It should be ascribed to the narrow interlayer distance, the formation of CuO , smaller grain size, and the high visible light absorption on the surface of $\text{Cu}^{2+}/\text{K}_2\text{La}_2\text{Ti}_3\text{O}_{10}$ calcined at 500 °C. It is found that the exposure of CO_2 could promote the photocatalytic activity of $\text{Cu}^{2+}/\text{K}_2\text{La}_2\text{Ti}_3\text{O}_{10}$. It also suggests that CO_2 is involved in the reduction to form benzaldehyde during decomposition of chlorobenzene.

Keywords: solar light; photocatalytic activity; chlorobenzene; layered perovskite; ion-exchange

1. Introduction

Volatile organic compounds (VOCs) were found to be toxic, malodorous, carcinogenic, mutagenic, and teratogenic to human health [1]. Among them, chlorobenzene is listed by the US Environmental Protection Agency as a priority pollutant [2]. Chlorobenzene as one of volatile organic compounds (VOCs) is widely used in the pharmaceutical industry as a solvent and in dye processes [3]. Figure 1 presents the framework of chlorobenzene. As one of bio-refractory and hydrophobic organics, it cannot be removed by biological treatment [2]. Presently, TiO_2 with a band gap of 3.2 eV has been the most accepted photocatalyst for decomposition of various pollutants, including refractory VOCs, due to its thermal stability, facile synthesis, low cost, and low toxicity [4]. However, the general drawbacks of TiO_2 as a photocatalyst, such as low reaction rates and limited response range toward light, require improvement [5,6]. Therefore, developing new types of photocatalysts with higher photocatalytic activity and visible-light response has received increasing interest.

In recent years, several layered perovskites, such as $\text{K}_2\text{La}_2\text{Ti}_3\text{O}_{10}$, $\text{Sm}_2\text{Ti}_2\text{S}_2\text{O}_5$, $\text{H}_4\text{Nb}_6\text{O}_{17}$ and $\text{Sr}_3\text{Ti}_2\text{O}_7$, have been considered to have photocatalytic activity [7–9]. The higher photocatalytic activity of the perovskites were ascribed to its specific layered structure. They use the interlayer space as reactions sites to separate the electron–hole pairs [6]. Moreover, the interlayer ions are ion-exchangeable with various foreign species to obtain photocatalysts with higher activity [4,10]. However, most

of the studies were mainly on photochemical splitting of water to produce hydrogen, there were a few reports on photocatalytic degradation of chlorobenzene, especially under simulant solar light irradiation. Benzaldehyde has been known to be formed from the photocatalytic degradation of chlorobenzene, which reacted with formaldehyde formed earlier [1]. On the other hand, gaseous CO₂ could be converted to formaldehyde by the photo reduction on photocatalyst. Formic acid, formaldehyde, methanol, and methane were detected as the CO₂ reduction products at a Cu electrode and nitrogen-doped TiO₂ thin film as a photoanode under illumination [11]. A successive double electron reduction of CO₂ to CH₃OH or CH₄ via CH₂O by photocatalysis was also considered [12]. Therefore, we think that CO₂ may improve the separation of electron-hole pairs and promote the degradation of chlorobenzene.

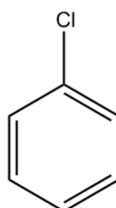


Figure 1. The framework of chlorobenzene.

In this paper, we synthesized the layered metal oxide, K₂La₂Ti₃O₁₀, with sol-gel method. The Cu²⁺/K₂La₂Ti₃O₁₀ powder was obtained by ion-exchange reaction with the original K₂La₂Ti₃O₁₀. The photocatalytic activity for chlorobenzene decomposition with K₂La₂Ti₃O₁₀ and Cu²⁺/K₂La₂Ti₃O₁₀ powders under simulated solar irradiation were investigated. We also discussed the influences of ion-exchange on physical and chemical properties of the prepared photocatalysts and the effects of CO₂ concentration on the photocatalytic activity of Cu²⁺/K₂La₂Ti₃O₁₀.

2. Results and Discussion

2.1. Characterization of the Powders

The UV-vis absorption spectra of original K₂La₂Ti₃O₁₀ and Cu²⁺/K₂La₂Ti₃O₁₀ calcined at different temperature are shown in Figure 2. In the present study, the sharp UV absorption edge of the original K₂La₂Ti₃O₁₀ is identified near 351 nm. However, ion-exchange of Cu²⁺ causes a red shift of the absorption edge and the Cu²⁺/K₂La₂Ti₃O₁₀ photocatalysts calcined at different temperature show different light response behaviors in the visible light range from 400 to 700 nm. Moreover, the highest visible light absorption appears on the surface of Cu²⁺/K₂La₂Ti₃O₁₀ calcined at 500 °C.

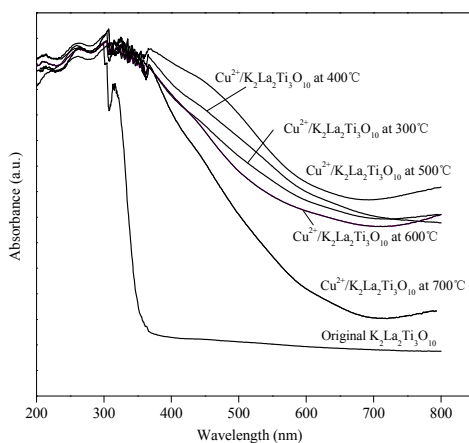


Figure 2. UV-Vis absorption spectra of original K₂La₂Ti₃O₁₀, Cu²⁺/K₂La₂Ti₃O₁₀ calcined at 300, 400, 500, 600 and 700 °C.

Figure 3 shows that the XRD patterns of $\text{Cu}^{2+}/\text{K}_2\text{La}_2\text{Ti}_3\text{O}_{10}$ and original $\text{K}_2\text{La}_2\text{Ti}_3\text{O}_{10}$ calcined at different temperatures. $\text{K}_2\text{La}_2\text{Ti}_3\text{O}_{10}$ is composed of negatively charge lanthanum titanium perovskite layers interleaved by K^+ ions and the adjacent triple perovskite sheets, $\text{La}_2\text{Ti}_3\text{O}_{10}$, are stacked with a displacement by $1/2$ along the (110) direction [13]. The interlayers are bonded by static force [6]. It belongs to the space group of $I4/mmm$ and symmetry of $C4v$, and the parameters of $\text{K}_2\text{La}_2\text{Ti}_3\text{O}_{10}$ cell are $a = b = 0.387$ nm, $c = 2.978$ nm [4,13,14]. In the present study, the powder X-ray diffraction pattern of the original $\text{K}_2\text{La}_2\text{Ti}_3\text{O}_{10}$ (Figure 3g–i) agreed well with the $\text{K}_2\text{La}_2\text{Ti}_3\text{O}_{10}$ crystal phase (PDF#48-0982). The distinctive peaks at $2\theta = 5.90^\circ, 11.84^\circ, 17.80^\circ, 23.12^\circ, 23.86^\circ, 24.62^\circ, 27.44^\circ, 31.20^\circ, 32.66^\circ, 37.46^\circ, 40.88^\circ, 42.46^\circ, 46.86^\circ, 48.88^\circ, 53.26^\circ, 54.58^\circ, 57.40^\circ$, corresponding to the $\text{K}_2\text{La}_2\text{Ti}_3\text{O}_{10}$ (0 0 2), (0 0 4), (0 0 6), (1 0 1), (0 0 8), (1 0 3), (1 0 5), (1 0 7), (1 1 0), (1 1 6), (1 1 8), (0 0 14), (2 0 0), (2 0 4), (2 1 1), (1 1 14), (2 1 7) crystal planes are observed in original $\text{K}_2\text{La}_2\text{Ti}_3\text{O}_{10}$ sample. The XRD pattern of original $\text{K}_2\text{La}_2\text{Ti}_3\text{O}_{10}$ calcined at 650°C (Figure 3f) shows weak characteristic lines, which indicates that it cannot form $\text{K}_2\text{La}_2\text{Ti}_3\text{O}_{10}$ structure when the precursor is calcined below 650°C . The peak positions of $\text{Cu}^{2+}/\text{K}_2\text{La}_2\text{Ti}_3\text{O}_{10}$ calcined at different temperatures are different from the original $\text{K}_2\text{La}_2\text{Ti}_3\text{O}_{10}$. Compared to original $\text{K}_2\text{La}_2\text{Ti}_3\text{O}_{10}$ sample, the $\text{Cu}^{2+}/\text{K}_2\text{La}_2\text{Ti}_3\text{O}_{10}$ samples show a significant shift of the (002) peak. There is no shift of the (002) peaks of original $\text{K}_2\text{La}_2\text{Ti}_3\text{O}_{10}$ with increase of calcination temperature (Figure 3g–i). By comparing the characteristic lines of Figure 3g–i with Figure 3a–e), it is found that the shift of (002) peak should be attributed to ion-exchange of Cu^{2+} , rather than the increase of calcination temperature. Moreover, the d values for the (002) reflection changes from 1.497 nm for the original $\text{K}_2\text{La}_2\text{Ti}_3\text{O}_{10}$ to 1.429 nm (300°C), 1.424 nm (400°C), 1.420 nm (500°C), 1.406 nm (600°C), and 1.415 nm (700°C) for the $\text{Cu}^{2+}/\text{K}_2\text{La}_2\text{Ti}_3\text{O}_{10}$ powders. It is clear from the above observation that Cu^{2+} ions is incorporated in place of K^+ ions. And the decrease in d (002) value and the peak shift possibly result from the smaller ion radius of Cu^{2+} (0.70 \AA) compared with that of K^+ (1.65 \AA) [4,10,15,16]. Furthermore, some weak peaks appeared at 38.80° and 53.78° for $\text{Cu}^{2+}/\text{K}_2\text{La}_2\text{Ti}_3\text{O}_{10}$ samples, which can be attributed to CuO (PDF#01-1117), become more obvious as the calcination temperature increases. However, the d value decreases, except for $\text{Cu}^{2+}/\text{K}_2\text{La}_2\text{Ti}_3\text{O}_{10}$ sample at 700°C . It indicates that, with the rise of the temperature, more interlayer Cu^{2+} is converted into new crystal phase CuO . The full widths at half maximum of $\text{Cu}^{2+}/\text{K}_2\text{La}_2\text{Ti}_3\text{O}_{10}$ samples are broader than that of original $\text{K}_2\text{La}_2\text{Ti}_3\text{O}_{10}$, indicating that the grain growth is inhibited by ion-exchange, which results in small grain size (Table 1). Surface characteristics of $\text{Cu}^{2+}/\text{K}_2\text{La}_2\text{Ti}_3\text{O}_{10}$ calcined at different temperatures and original $\text{K}_2\text{La}_2\text{Ti}_3\text{O}_{10}$ samples measured by N_2 adsorption are summarized in Table 1. After ion-exchange reaction, the specific surface areas of $\text{Cu}^{2+}/\text{K}_2\text{La}_2\text{Ti}_3\text{O}_{10}$ calcined at different temperature are higher than the original $\text{K}_2\text{La}_2\text{Ti}_3\text{O}_{10}$ sample, ranging from 2.7 to $5.8 \text{ m}^2/\text{g}$. Table 1 also shows the chlorobenzene degradation ratio of $\text{Cu}^{2+}/\text{K}_2\text{La}_2\text{Ti}_3\text{O}_{10}$ calcined at different temperatures and original $\text{K}_2\text{La}_2\text{Ti}_3\text{O}_{10}$. It was found that degradation ratio of $\text{Cu}^{2+}/\text{K}_2\text{La}_2\text{Ti}_3\text{O}_{10}$ at 500°C reached to 51.1%, about 16.9% higher than that of the original $\text{K}_2\text{La}_2\text{Ti}_3\text{O}_{10}$ (34.2%). It should be ascribed to the narrow interlayer distance, the formation of CuO , and smaller grain size [17–19]. The unique structure of layered perovskite and the heterojunction between the CuO and the perovskite are in favor of the separation of electron-hole pairs for higher photocatalytic activity. With the increase of calcination temperature, the degradation ratio increase and reach the maximum at 500°C . It results from the high visible light absorption on the surface of $\text{Cu}^{2+}/\text{K}_2\text{La}_2\text{Ti}_3\text{O}_{10}$ calcined at 500°C (Figure 2), except for narrow interlayer distance and the formation of CuO . However, excessive calcination temperature decreases the photocatalytic activity, which is ascribed to the lower specific surface area (Table 1) and low visible light absorption.

Figure 4 presents the comparison of photocatalytic activity of $\text{Cu}^{2+}/\text{K}_2\text{La}_2\text{Ti}_3\text{O}_{10}$ with other ions exchanged $\text{K}_2\text{La}_2\text{Ti}_3\text{O}_{10}$ (Ni^{2+} , Sn^{2+} , Ce^{2+} and Fe^{2+}). The degradation ratio order for chlorobenzene is $\text{Cu}^{2+}/\text{K}_2\text{La}_2\text{Ti}_3\text{O}_{10} > \text{Fe}^{2+}/\text{K}_2\text{La}_2\text{Ti}_3\text{O}_{10} > \text{Ce}^{2+}/\text{K}_2\text{La}_2\text{Ti}_3\text{O}_{10} > \text{Sn}^{2+}/\text{K}_2\text{La}_2\text{Ti}_3\text{O}_{10} > \text{Ni}^{2+}/\text{K}_2\text{La}_2\text{Ti}_3\text{O}_{10}$. The degradation ratios of the last three catalysts for chlorobenzene are even less than that of the original $\text{K}_2\text{La}_2\text{Ti}_3\text{O}_{10}$.

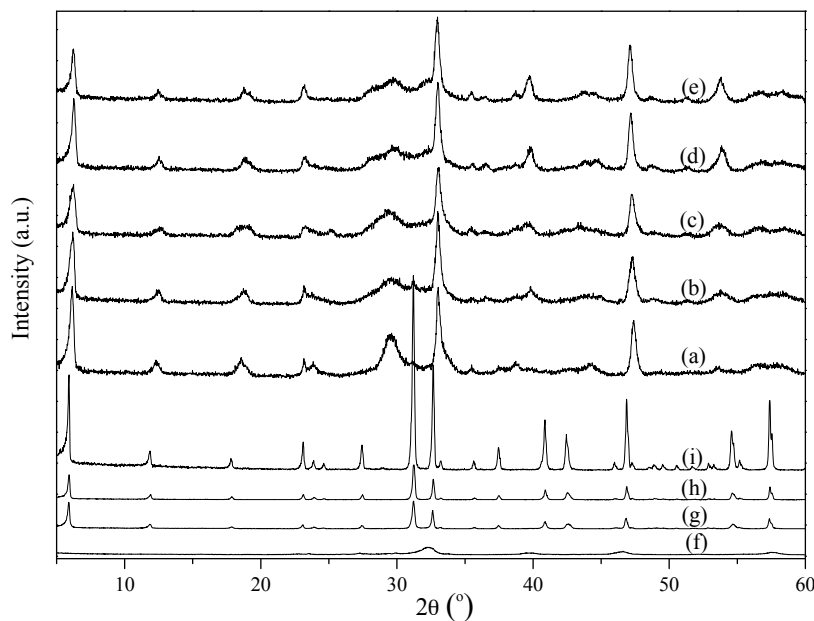


Figure 3. XRD patterns of $\text{Cu}^{2+}/\text{K}_2\text{La}_2\text{Ti}_3\text{O}_{10}$ calcined at 300 °C (a), 400 °C (b), 500 °C (c), 600 °C (d), 700 °C (e); and original $\text{K}_2\text{La}_2\text{Ti}_3\text{O}_{10}$ calcined at 650 °C (f), 750 °C (g), 850 °C (h), 950 °C (i).

Table 1. Grain size, specific surface area, and chlorobenzene degradation ratio of $\text{Cu}^{2+}/\text{K}_2\text{La}_2\text{Ti}_3\text{O}_{10}$ at different calcination temperatures and original $\text{K}_2\text{La}_2\text{Ti}_3\text{O}_{10}$ in air.

Samples	Grain Size (nm) ^a	Specific Surface Area (m ² /g)	Degradation Ratio (%)
Original $\text{K}_2\text{La}_2\text{Ti}_3\text{O}_{10}$ at 950 °C	61.8	2.0	34.2
$\text{Cu}^{2+}/\text{K}_2\text{La}_2\text{Ti}_3\text{O}_{10}$ at 300 °C	13.0	5.8	46.0
$\text{Cu}^{2+}/\text{K}_2\text{La}_2\text{Ti}_3\text{O}_{10}$ at 400 °C	15.5	5.0	48.0
$\text{Cu}^{2+}/\text{K}_2\text{La}_2\text{Ti}_3\text{O}_{10}$ at 500 °C	13.0	4.6	51.1
$\text{Cu}^{2+}/\text{K}_2\text{La}_2\text{Ti}_3\text{O}_{10}$ at 600 °C	13.8	3.4	45.0
$\text{Cu}^{2+}/\text{K}_2\text{La}_2\text{Ti}_3\text{O}_{10}$ at 700 °C	20.3	2.7	44.0

^a According to Scherrer equation, the grain size was calculated from the full width at half maximum of the peak at 23.12°.

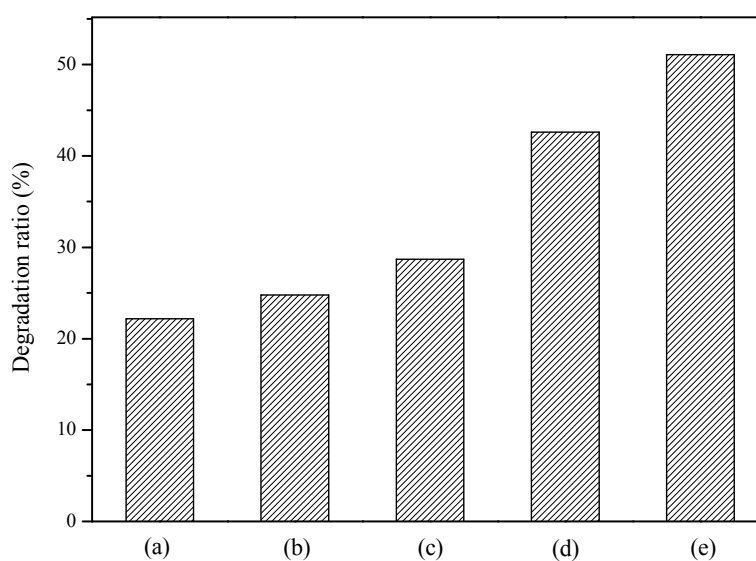


Figure 4. Comparison of photocatalytic activities with: (a) $\text{Ni}^{2+}/\text{K}_2\text{La}_2\text{Ti}_3\text{O}_{10}$; (b) $\text{Sn}^{2+}/\text{K}_2\text{La}_2\text{Ti}_3\text{O}_{10}$; (c) $\text{Ce}^{2+}/\text{K}_2\text{La}_2\text{Ti}_3\text{O}_{10}$; (d) $\text{Fe}^{2+}/\text{K}_2\text{La}_2\text{Ti}_3\text{O}_{10}$; and (e) $\text{Cu}^{2+}/\text{K}_2\text{La}_2\text{Ti}_3\text{O}_{10}$.

2.2. Effect of Initial Concentration on the Photocatalytic Activity

Figure 5 presents the relationship between the initial concentration of chlorobenzene and the degradation ratio. It is observed that the degradation ratio increases with the initial concentration increase of chlorobenzene up to 13.3 $\mu\text{g}/\text{mL}$. When the initial concentration exceeds this value, the degradation ratio decreases. With the rise of initial concentration, the active sites will be covered by chlorobenzene [20], which may decrease the degradation ratio due to the loss of active sites. Moreover, based on the results of Zhang [21], the intermediates (*o*-, *m*-, *p*-chlorophenol) are likely to accumulate on the surface of the photocatalyst during the photocatalytic degradation of chlorobenzene, which will lead to a decrease in the degradation ratio with irradiation time.

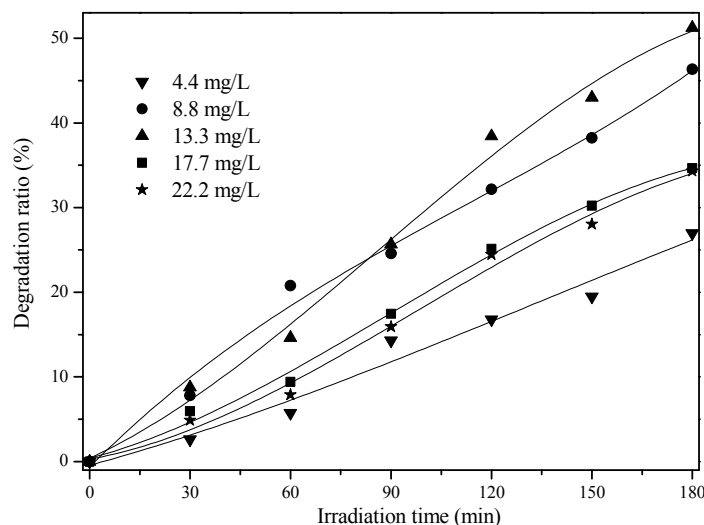


Figure 5. Effect of initial concentration on the degradation of chlorobenzene with $\text{Cu}^{2+}/\text{K}_2\text{La}_2\text{Ti}_3\text{O}_{10}$.

2.3. Effect of CO_2 Concentration on the Photocatalytic Activity

In order to investigate the effect of CO_2 concentration on the photocatalytic activity, the reactor was purged by 100% N_2 , 70% N_2 + 30% CO_2 , 50% N_2 + 50% CO_2 , 30% N_2 + 70% CO_2 , and 100% CO_2 for 30 min to fill the reactor and the other experiment conditions were the same as those in photocatalytic experiments. Figure 6 shows the effect of CO_2 concentration on the chlorobenzene degradation ratio of $\text{Cu}^{2+}/\text{K}_2\text{La}_2\text{Ti}_3\text{O}_{10}$ at 500 $^\circ\text{C}$. The degradation ratio is lower (only 48%) under simulant solar light irradiation for 180 min in the absence of CO_2 . After CO_2 is introduced, the degradation ratio increase with the CO_2 concentration. It can reach 68% at 50% CO_2 + 50% N_2 . The apparent rate constant (min^{-1}) (K_{app}) and corresponding correlation coefficient (R^2) is also calculated according to the pseudo-first-order equation [22], as shown in Table 2. Figure 7 shows the chlorobenzene degradation ratio and apparent rate constant of $\text{Cu}^{2+}/\text{K}_2\text{La}_2\text{Ti}_3\text{O}_{10}$ at 500 $^\circ\text{C}$ as a function of CO_2 concentration. With the increase of the CO_2 concentration, the degradation ratio rises and then decreases. The apparent rate constant follows a similar trend. It demonstrates that the exposure of CO_2 can improve the photocatalytic activity of $\text{Cu}^{2+}/\text{K}_2\text{La}_2\text{Ti}_3\text{O}_{10}$. However, excessive CO_2 concentration can decrease the photocatalytic activity of $\text{Cu}^{2+}/\text{K}_2\text{La}_2\text{Ti}_3\text{O}_{10}$, and the reason is still not clear. Further in-depth experiments would be required to clearly understand the reason of the lower activity of $\text{Cu}^{2+}/\text{K}_2\text{La}_2\text{Ti}_3\text{O}_{10}$ with excessive CO_2 concentration.

As one of bio-refractory organics, heterogeneous photocatalytic oxidation and other advanced oxidation processes have been developed to remove chlorobenzene. Dilmeghani and Zahir reported that the observed pseudo first-order rate constants in air-saturated solution, oxygen-saturated solution, and under anaerobic condition are 5.1×10^{-4} , 6.4×10^{-4} , and $1.8 \times 10^{-4} \text{ s}^{-1}$ for UV-induced degradation of chlorobenzene with pH value at 3.5 [23]. Tseng et al. reported that 42.8%

of monochlorobenzene was degraded under UV light irradiation for 240 min, and the extent of monochlorobenzene degradation within 240 min of UV irradiation was approximately 60.2%, under the condition of H_2O_2 dosage equal to 22.5 mg/L [24]. The rate constant of monochlorobenzene degradation in UV/ TiO_2/O_2 photocatalysis was increased from 0.016 to 0.046 min^{-1} , as the initial concentration of dissolved oxygen (DO) was increased from 1.6 to 28.3 mg/L [24]. The apparent rate constant of $\text{Cu}^{2+}/\text{K}_2\text{La}_2\text{Ti}_3\text{O}_{10}$ during the photocatalytic degradation of chlorobenzene is $1.1 \times 10^{-4} \text{ s}^{-1}$ and $6.8 \times 10^{-5} \text{ s}^{-1}$ (corresponding to degradation ratio of 67.8% and 51.1%) under the reactor filled with 50% $\text{CO}_2 + 50\% \text{ N}_2$ and air, respectively. $\text{Cu}^{2+}/\text{K}_2\text{La}_2\text{Ti}_3\text{O}_{10}$ exhibits high photocatalytic activity for chlorobenzene degradation under simulated solar light irradiation, rather than UV light, and without H_2O_2 .

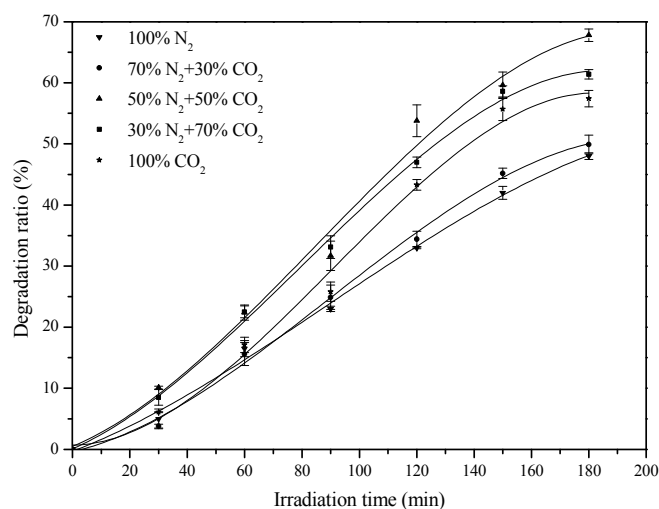


Figure 6. Effect of CO_2 concentration on the chlorobenzene degradation ratio of $\text{Cu}^{2+}/\text{K}_2\text{La}_2\text{Ti}_3\text{O}_{10}$ at 500 °C.

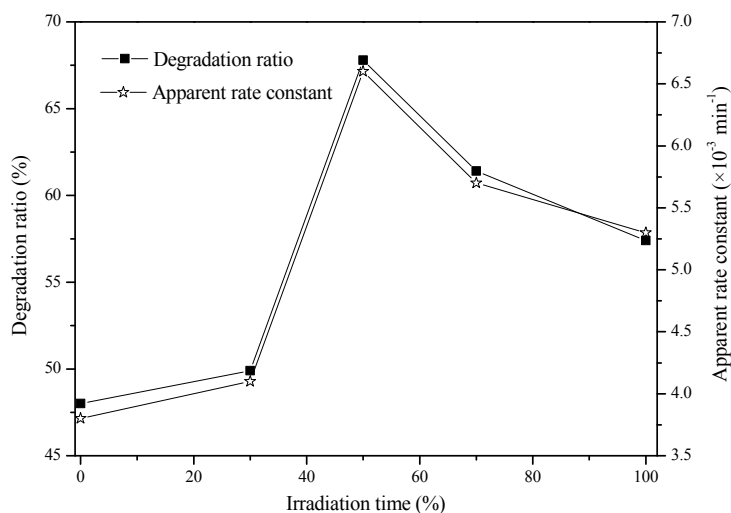


Figure 7. Chlorobenzene degradation ratio and apparent rate constant of $\text{Cu}^{2+}/\text{K}_2\text{La}_2\text{Ti}_3\text{O}_{10}$ at 500 °C as a function of CO_2 concentration.

Formaldehyde is an important product of the photoreduction of gaseous CO_2 on semiconductor-based photocatalysis [25]. Based on literatures [1,12,25,26], a pathway might occur during the photocatalytic degradation of chlorobenzene. Dimitrijevic et al. have found that CO_2 could be reduced to CH_3O radical and HCOOH on titania under UV illumination [26]. CH_2O (or HCHO)

was generated from the interaction between HCOOH and hydrogen radicals (H^\bullet) [11] or the interaction between HCOOH, H^+ and e^-_{CB} during CO_2 reduction on titania under illumination [25,26]. Moreover, we found formaldehyde generation by photo degradation of chlorobenzene on $Zn/KLaTi_2O_6$ photocatalyst, and then chlorobenzene converted to benzaldehyde by dechlorination and reaction with formaldehyde formed earlier [1]. In this paper, the chlorobenzene degradation ratio increases with the CO_2 concentration on $Cu^{2+}/K_2La_2Ti_3O_{10}$. It implies that benzaldehyde was similarly generated through reaction with formaldehyde (HCOH) intermediate during CO_2 reduction in the photocatalytic reaction on $Cu^{2+}/K_2La_2Ti_3O_{10}$, which is in favor of the immobilization of greenhouse gases CO_2 .

Table 2. Degradation ratio, apparent rate constant, and correlation coefficient (R^2) of chlorobenzene with $Cu^{2+}/K_2La_2Ti_3O_{10}$ at 500 °C under different CO_2 concentrations.

Irradiation Time (min)	Degradation Ratio (%)							Apparent Rate Constant (min^{-1})	R^2
	0	30	60	90	120	150	180		
100% N_2	0	5	16.5	23.0	33.0	42.0	48.0	0.0038	0.9882
70% N_2 + 30% CO_2	0	3.8	15.6	24.9	34.4	45.2	49.9	0.0041	0.9836
50% N_2 + 50% CO_2	0	10.1	22.4	31.7	53.8	59.6	67.8	0.0066	0.9714
30% N_2 + 70% CO_2	0	8.5	22.5	33.1	47.0	58.6	61.4	0.0057	0.9823
100% CO_2	0	6.1	17.1	25.8	43.3	55.7	57.4	0.0053	0.9601

3. Experimental

3.1. Preparation of Photocatalysts

The $K_2La_2Ti_3O_{10}$ powder was prepared by sol-gel process. 0.02 mol $La(NO_3)_3 \cdot nH_2O$ and 0.04 mol KNO_3 were dissolved in 22 mL water to form solution A. 0.03 mol titanium tetrabutyl ($Ti(OC_4H_9)_4$) was dissolved in 80 mL isopropanol ($(CH_3)_2CHOH$) with stirring for 30 min to form solution B. Solution A was added dropwise into solution B with vigorous stirring for 20 min to get the gelatinous solution. The resulted gelatinous solution was aged for 12 h at room when water and isopropanol were separated from the gel. The gel was then dried at 80 °C, crushed and calcined under different calcination temperatures for 4 h to obtain original $K_2La_2Ti_3O_{10}$ powder.

The $Cu^{2+}/K_2La_2Ti_3O_{10}$ powder was synthesized by ion-exchange reaction. The original $K_2La_2Ti_3O_{10}$ powder at 950 °C (1 g) was added into 0.1 mol/L $Cu(NO_3)_2$ aqueous solution (100 mL). The solution was maintained at 333 K for two days. The sample after washing with distilled water to remove Cu^{2+} adsorbed on the surface of the sample was dried at room temperature and calcined at 300, 400, 500, 600, and 700 °C for 2 h to obtain $Cu^{2+}/K_2La_2Ti_3O_{10}$ powder.

For comparison, $Ni^{2+}/K_2La_2Ti_3O_{10}$, $Sn^{2+}/K_2La_2Ti_3O_{10}$, $Ce^{2+}/K_2La_2Ti_3O_{10}$, and $Fe^{2+}/K_2La_2Ti_3O_{10}$ were also synthesized by the same ion-exchange reaction of the original $K_2La_2Ti_3O_{10}$ with 0.1 mol/L $Ce(NO_3)_3$, $Ni(NO_3)_2$, $SnCl_2$, and $Fe(NO_3)_3$, respectively.

3.2. Characterization of Photocatalysts

The X-ray diffraction (XRD, Rigaku Corporation, Tokyo, Japan) patterns of the powders were obtained on a Rigaku D/max 2500 X-ray diffraction analyzer with $Cu K\alpha$ X-ray source at a scanning rate of $8^\circ/min$ in the 2θ range between 5° and 80° . The accelerating voltage and the applied current were 40 kV and 200 mA, respectively. The specific surface area of samples was measured by nitrogen gas adsorption at 77 K using an automated adsorption apparatus (BELSOROP-MINI II). UV-visible diffuse reflectance spectroscopy of the powders was collected with Shimadzu Corporation UV-2540 (Kyoto, Japan) over the spectral range 240–800 nm. $BaSO_4$ was used as a reference.

3.3. Photocatalytic Experiments

Photocatalytic reaction was carried out in a self-made cylindroid glass reactor using a 350 W xenon arc lamp (ShenZhen AnHongDa Opto Technology Co., Ltd., Shenzhen, China) with similar

characteristic spectrum with sun light as a light source of simulant solar light. A typical experiment of degradation was carried out as follows: a suspension containing 13.23 g/L the catalyst in distilled water was prepared. The surface of a frosted glass plate (25.0×53.0 mm, 13.25 cm²) was cleaned with acetone. The suspension was poured on the glass plate and then it was dried at 110 °C. Deposition process was performed four times to obtain a catalyst loading density of 3.77×10^{-2} g/cm², as estimated by weighing the plate before and after the deposition process. The plate was dried at 110 °C and placed at the center of the reactor. 1 μL chlorobenzene liquid was injected into the sealed reactor filled with air and allowed to evaporate with a small magnetic stirring fan. Illumination was initialized after it got to adsorption equilibrium. The small fan guaranteed the gases circulated inside the reactor. 500 μL gases was withdrawn from the reactor with a syringe periodically and further analyzed by gas chromatography (SP-6890, Shandong Lunan Ruihong Chemical Instruments Co., Ltd., Tengzhou, China) to obtain the chlorobenzene concentration. All of the tests were conducted at the room temperature (298 K). Each degradation experiment was repeated three times. The degradation ratios at different irradiation times of three parallel experiments were determined using degradation ratio equation [22] and the corresponding chlorobenzene concentration. The average value and standard deviation of the degradation ratio of parallel experiments were taken as the final degradation ratio and error bars.

The photocatalytic activity for chlorobenzene decomposition with different initial concentration of chlorobenzene were investigated by varying the amount of chlorobenzene liquid injected into the reactor, and the initial concentrations of chlorobenzene were quantified by GC.

4. Conclusions

In summary, original $K_2La_2Ti_3O_{10}$ and $Cu^{2+}/K_2La_2Ti_3O_{10}$ were successfully prepared. The XRD analysis demonstrates that Cu^{2+} ions are incorporated in place of K^+ ions. With the rise of calcination temperature, more interlayer Cu^{2+} was converted into new crystal phase CuO. The degradation ratio of $Cu^{2+}/K_2La_2Ti_3O_{10}$ is improved after ion-exchange, which should be ascribed to the narrow interlayer distance, the formation of CuO, smaller grain size, and the high visible light absorption on the surface of $Cu^{2+}/K_2La_2Ti_3O_{10}$ calcined at 500 °C. Moreover, the exposure of CO_2 can improve the photocatalytic activity of $Cu^{2+}/K_2La_2Ti_3O_{10}$.

Acknowledgments: This project was financially supported by Foundation Science and Technology innovation Committee of Shenzhen, China (JCYJ20150731104949798, ZDSYS201603301417558) and National Natural Science Foundation of China (71371060).

Author Contributions: Dandan Pang and Feng Ouyang conceived and designed the experiments; Dandan Pang and Jie Gao analyzed the data; Rongshu Zhu and Charlene Xie contributed reagents, materials and analysis tools; Dandan Pang wrote the paper.

Conflicts of Interest: The authors declare no conflict of interest.

References

1. Pang, D.; Dong, M.; Ma, X.; Ouyang, F. Photocatalytic decomposition of gas-phase chlorobenzene with transition metal-doped $KLaTi_2O_6$ under visible light irradiation. *Environ. Eng. Sci.* **2014**, *31*, 1–8. [[CrossRef](#)]
2. Cheng, Z.; Gu, Z.; Chen, J.; Yu, J.; Zhou, L. Synthesis, characterization, and photocatalytic activity of porous La-N-co-doped TiO_2 nanotubes for gaseous chlorobenzene oxidation. *J. Environ. Sci. China* **2016**, *46*, 203–213. [[CrossRef](#)] [[PubMed](#)]
3. Zhu, R.; Mao, Y.; Jiang, L.; Chen, J. Performance of chlorobenzene removal in a nonthermal plasma catalysis reactor and evaluation of its byproducts. *Chem. Eng. J.* **2015**, *279*, 463–471. [[CrossRef](#)]
4. Kumar, V.; Govind; Uma, S. Investigation of cation (Sn^{2+}) and anion (N^{3-}) substitution in favor of visible light photocatalytic activity in the layered perovskite $K_2La_2Ti_3O_{10}$. *J. Hazard. Mater.* **2011**, *189*, 502–508. [[CrossRef](#)] [[PubMed](#)]
5. Hsieh, C.; Lai, M.; Pan, C. Synthesis and visible-Light-Derived photocatalysis of titania nanosphere stacking layers prepared by chemical vapor deposition. *J. Chem. Technol. Biotechnol.* **2010**, *85*, 1168–1174. [[CrossRef](#)]

6. Huang, Y.; Wei, Y.; Cheng, S.; Fan, L.; Li, Y.; Lin, J.; Wu, J. Photocatalytic property of nitrogen-Doped layered perovskite $K_2La_2Ti_3O_{10}$. *Sol. Energy Mater. Sol. C* **2010**, *94*, 761–766. [[CrossRef](#)]
7. Liu, L.; Guo, D.; Cui, W.; Hu, J.; Liang, Y. Photocatalytic hydrogen evolution from the splitting of water over $Cd_{1-x}Zn_xS/K_2La_2Ti_3O_{10}$ composites under visible light irradiation. *J. Wuhan Univ. Technol.* **2015**, *30*, 928–934. [[CrossRef](#)]
8. Osterloh, F.E. Inorganic materials as catalysts for photochemical splitting of water. *Chem. Mater.* **2008**, *20*, 35–54. [[CrossRef](#)]
9. Abe, R.; Shinmei, K.; Koumura, N.; Hara, K.; Ohtani, B. Visible-Light-Induced water splitting based on two-Step photoexcitation between dye-Sensitized layered niobate and tungsten oxide photocatalysts in the presence of a triiodide/iodide shuttle redox mediator. *J. Am. Chem. Soc.* **2013**, *135*, 16872–16884. [[CrossRef](#)] [[PubMed](#)]
10. Uma, S.; Singh, J.; Thakral, V. Facile room temperature ion-Exchange synthesis of Sn^{2+} incorporated pyrochlore-type oxides and their photocatalytic activities. *Inorg. Chem.* **2009**, *48*, 11624–11630. [[CrossRef](#)] [[PubMed](#)]
11. Peng, Y.; Yeh, Y.; Shah, S.I.; Huang, C.P. Concurrent photoelectrochemical reduction of CO_2 and oxidation of methyl orange using nitrogen-Doped TiO_2 . *Appl. Catal. B Environ.* **2012**, *123–124*, 414–423. [[CrossRef](#)]
12. Ulagappan, N.; Frei, H. Mechanistic study of CO_2 photoreduction in Ti silicalite molecular sieve by FT-IR spectroscopy. *J. Phys. Chem. A* **2000**, *104*, 7834–7839. [[CrossRef](#)]
13. Toda, K.; Watanabe, J.; Sato, M. Crystal structure determination of ion-Exchangeable layered perovskite compounds, $K_2La_2Ti_3O_{10}$ and $Li_2La_2Ti_5O_{10}$. *Mater. Res. Bull.* **1996**, *31*, 1427–1435. [[CrossRef](#)]
14. Yang, Y.-H.; Chen, Q.-Y.; Yin, Z.-L.; Li, J. Study on the photocatalytic activity of $K_2La_2Ti_3O_{10}$ doped with zinc(Zn). *Appl. Surf. Sci.* **2009**, *255*, 8419–8424.
15. Yavuz, O.; Altunkaynak, Y.; Guzel, F. Removal of copper, nickel, cobalt and manganese from aqueous solution by kaolinite. *Water Res.* **2003**, *37*, 948–952. [[CrossRef](#)]
16. Dean, J.A. *Lang's Handbook of Chemistry*; McGraw-Hill, Inc.: New York, NY, USA, 1991; p. 319.
17. Kitano, M.; Hara, M. Heterogeneous photocatalytic cleavage of water. *J. Mater. Chem.* **2010**, *20*, 627–641. [[CrossRef](#)]
18. Zhang, Z.; Huang, J.; Zhang, M.; Yuan, Q.; Dong, B. Ultrathin hexagonal SnS_2 nanosheets coupled with $g-C_3N_4$ nanosheets as 2D/2D heterojunction photocatalysts toward high photocatalytic activity. *Appl. Catal. B Environ.* **2015**, *163*, 298–305. [[CrossRef](#)]
19. Pang, D.; Qiu, L.; Zhu, R.; Ouyang, F. Silica supported SO_4^{2-}/TiO_2 for photocatalytic decomposition of acrylonitrile under simulant solar light irradiation. *Chem. Eng. J.* **2015**, *270*, 590–596. [[CrossRef](#)]
20. Sakthivel, S.; Neppolian, B.; Shankar, M.V.; Arabindoo, B.; Palanichamy, M.; Murugesan, V. Solar photocatalytic degradation of azo dye: Comparison of photocatalytic efficiency of ZnO and TiO_2 . *Sol. Energy Mater. Sol. Cell* **2003**, *77*, 65–82. [[CrossRef](#)]
21. Zhang, L.; Sawell, S.; Moralejo, C.; Anderson, W. Heterogeneous photocatalytic decomposition of gas-Phase chlorobenzene. *Appl. Catal. B Environ.* **2007**, *71*, 135–142. [[CrossRef](#)]
22. Pang, D.; Wang, Y.; Ma, X.; Ouyang, F. Fluorine promoted and silica supported TiO_2 for photocatalytic decomposition of acrylonitrile under simulant solar light irradiation. *Chem. Eng. J.* **2014**, *258*, 43–50. [[CrossRef](#)]
23. Dilmeghani, M.; Zahir, K. Kinetics and mechanism of chlorobenzene degradation in aqueous samples using advanced oxidation processes. *J. Environ. Qual.* **2001**, *30*, 2062–2070. [[CrossRef](#)] [[PubMed](#)]
24. Tseng, D.; Juang, L.; Huang, H. Effect of oxygen and hydrogen peroxide on the photocatalytic degradation of monochlorobenzene in aqueous suspension. *Int. J. Photoenergy* **2012**, *2012*, 1–9. [[CrossRef](#)]
25. Fan, W.; Zhang, Q.; Wang, Y. Semiconductor-Based nanocomposites for photocatalytic H_2 production and CO_2 conversion. *Phys. Chem. Chem. Phys.* **2013**, *15*, 2632–2649. [[CrossRef](#)] [[PubMed](#)]
26. Dimitrijevic, N.M.; Vijayan, B.K.; Poluektov, O.G.; Rajh, T.; Gray, K.A.; He, H.; Zapol, P. Role of water and carbonates in photocatalytic transformation of CO_2 to CH_4 on titania. *J. Am. Chem. Soc.* **2011**, *133*, 3964–3971. [[CrossRef](#)] [[PubMed](#)]

